Materials Science & Engineering A 651 (2016) 854–858

Contents lists available at ScienceDirect

Materials Science & Engineering A

journal homepage: www.elsevier.com/locate/msea

Short communication

Improvement of aging kinetics and precipitate size refinement in Mg–Sn alloys by hafnium additions

S. Behdad [a], L. Zhou [b], H.B. Henderson [c], M.V. Manuel [c], Y. Sohn [b], A. Agarwal [a], B. Boesl [a,*]

[a] Department of Mechanical and Materials Engineering, Florida International University, Miami, FL 33174, USA
[b] Department of Materials Science and Engineering and Advanced Materials Processing and Analysis Center, University of Central Florida, Orlando, FL 32816, USA
[c] Department of Materials Science and Engineering, University of Florida, Gainesville, FL 32611, USA

ARTICLE INFO

Article history:
Received 17 July 2015
Received in revised form
13 November 2015
Accepted 14 November 2015

Keywords:
Magnesium alloys
Precipitation
Micro-alloying
Transmission electron microscopy (TEM)

ABSTRACT

Two Mg–Sn alloys were microalloyed by addition of Hafnium and their age-hardening response was studied at 200 °C. Time to reach peak hardness was significantly reduced and improved by Hf addition. TEM study showed Hf clusters in the close vicinity and at the surface of Mg_2Sn precipitates, which confirms that Hf clusters act as additional nucleation centers for Mg_2Sn precipitate formation. Our results support the validity of thermokinetic criterion proposed by Mendis for selection of microalloying elements in order to refine precipitate size, accelerate aging kinetics and enhance peak hardness.

1. Introduction

Magnesium (Mg) is a low-density structural material and the eighth most abundant element on earth. It can be machined faster and with less power than aluminum [1], as well as recycled at 5% of initial energy requirements for its extraction [2]. These properties have led to an increased attention to development of Mg alloys for applications where potential weight savings can be beneficial such as automotive [3,4], aerospace [5–7], and biomedical sectors [8–11].

The major hurdle in further utilization of Mg is the lack of an affordable magnesium alloy that exhibits proper creep and corrosion resistance at elevated temperatures (> 125 °C). Current benchmark Mg alloys are mainly of Mg–Al alloy family, i.e. AZ91D, AM50A, and AM60B [12]. However, the discontinuous β-$Mg_{17}Al_{12}$ precipitate formed near grain boundaries in these alloys is not thermally stable above 125 °C [13]. The main current alternative for elevated temperature applications is AE42, which can be used at service temperatures up to 170 °C [14]. Above this temperature, decomposition of the interdendritic lamellar phase $Al_{11}RE_3$ leads to an abrupt degradation of creep resistance [14,15]. Rare earths have also been added to Mg–Zn alloys to improve their mechanical properties at elevated temperatures [16–19]. These efforts have led to development of MEZ alloy which has better creep resistance than AE42 in 150–175 °C temperature range [20]. At temperatures up to 300 °C, Yttrium containing Mg alloys exhibit very good creep resistance and a corrosion performance on par with high purity aluminum alloys [21,22]. Despite their superior properties, application of commercially available Mg–Y–RE alloys, i.e. WE43 and WE54, has been limited to aerospace, F1 racing cars, and motor sports where added benefits can compensate for the economic disadvantage [20,23]. Relatively high cost of rare earths is the main drawback that limits applications of all of the above-mentioned alloy families. Mg–Sn alloys can potentially fill the gap in the market for an affordable Mg alloy that exhibits comparable performance.

Mg–Sn alloy system can be an excellent candidate for elevated temperature applications. It forms Mg_2Sn precipitate with a melting point of 770 °C, even higher than the melting point of the intermetallics formed in binary Mg–Gd, Mg–Y, and Mg–RE counterparts [24]. However, the precipitation process by artificial aging below 300 °C does not develop any metastable phases and the precipitates in Mg–Sn binary alloy are very coarse compared to other precipitate forming Mg alloys [25]. Previous research has shown that micro-alloying by other elements can remedy this issue [26–31].

Sasaki et al. [26] chose Zn as micro-alloying element and showed that addition of 0.1 and 0.5 at% Zn to Mg–2.2Sn reduces time to reach maximum hardness and increases peak hardness through refining precipitate size and dispersion during aging at 180 °C. Also in Mg–2.2Sn–0.5Zn, number density of newly formed rod-like precipitates on non-basal planes and plate shaped precipitates on the basal plane was increased.

* Corresponding author.
E-mail address: bboesl@fiu.edu (B. Boesl).

http://dx.doi.org/10.1016/j.msea.2015.11.043
0921-5093/

Mendis et al. [27] suggested a qualitative "thermo-kinetic" criterion for selection of micro-alloying elements and tested their hypothesis on the model Mg–Sn system. Based on this criterion, an element can refine precipitate size distribution if it satisfies the following three conditions: 1. Micro-alloying element (called X hereafter) has a tendency to phase separate from Mg matrix so that it can form heterogeneities that act as nucleation centers for precipitate formation. 2. Micro-alloyed element and Sn must not have repulsive tendencies, and 3. Heterogeneity formation of this micro-alloyed element should happen at lesser spatial distance and faster time scale than parent binary alloy without the micro-alloying element. Due to the lack of experimentally determined or calculated thermodynamic data for the three-component systems studied, binary phase diagrams were used for element selection. The presence of a large miscibility gap in Mg–X binary phase diagram, absence of miscibility gaps in Sn–X binary phase diagram, and estimated diffusivity values of X in Mg were used respectively as approximate measures for the three proposed conditions. Na was finally selected as the best micro-alloying element for Mg–Sn. It was concluded that Na addition increases number density of precipitates by two orders of magnitude and reduces the time to reach peak hardness from about 1000 to 58 h. Mg–1.3Sn–0.15 Na also had a 2.7-fold increase in hardness increment over Mg–1.3Sn binary alloy. Basal lath precipitates' mean length, width and thickness were reduced from 1500 nm to 230 nm, from 500 nm to 90, and from 54 nm to 25 nm respectively.

Mendis et al. [28] alloyed Mg–1.3Sn with Zn and Na additions and aged the resultant alloys at 200 °C. Adding 1.2 at% Zn showed some influence on time to reach peak hardness and number density of the precipitates, and most importantly changed particle morphology and thereby increased hardening increment significantly by approximately 300%. Mg–1.3Sn–1.2Zn–0.13 Na reached its peak hardness 30 times faster than parent Mg–1.3Sn alloy and number density of precipitates were increased by almost two orders of magnitude. The authors concluded that while Na and Zn both improve the hardening response of Mg–Sn binary alloy, the underlying mechanisms for these improvements are different. While Na acts by increasing the number density of precipitates, Zn additions change the particle morphology with respect to basal planes. The source of observed synergistic enhancement on precipitate refinement and aging kinetics remains unidentified, but it was suggested that reduction of interfacial energy, due to segregation at the interface, decreases the driving force for coarsening of the precipitates.

The present study is focused on modifying Mg–Sn alloys with Hf addition. Hafnium satisfies the three conditions proposed by Mendis' criterion based on available binary phase diagrams of the Mg–Hf and Hf–Sn systems [32,33]. Previous studies of mechanical properties and creep resistance of Mg–Sn alloys containing 1–10 wt% Sn (~0.2–2.3 at%) reported that 5 wt% Sn alloy (T5) showed the best tensile strength, while 10 wt% added Sn (T10) had the highest hardness and better creep resistance than AE42 at 150 °C [34]. Therefore, these two compositions were chosen and the effect of Hf additions to them was studied.

2. Materials and methods

A total of six alloys were made from high purity Mg chips (99.98 pct, Sigma-Aldrich), Tin powder (99.85 pct, Alfa-Aesar), and Hafnium powder (99.6 pct, Alfa-Aesar). Nominal compositions of the samples in both at% and wt% are listed in Table 1. Hereafter, all samples are described in wt%. All alloys were measured, mixed and cast under high purity Argon atmosphere in a glove box. Oxygen levels were monitored to be less than 10 ppm to prevent oxidation. Alloys were fabricated by melting in a resistance-heating furnace at 750 °C. Molten mixture was stirred with a graphite rod after 30 min to ensure proper mixing, and was cast after another 15 min in a graphite mold. Alloys were cut into small pieces and put in quartz tubes. Tubes were vacuumed and then partially pressurized with Ar and sealed for homogenization treatment. For homogenization, alloys were heated to 345 °C at a heating rate of 80 °C/h and kept at that temperature for 2 h, then heated to 500 °C at 80 °C/h rate and kept for 6 h at 500 °C. Samples were then quenched in cold water. After homogenization, age hardening behavior of the samples was studied by artificial ageing in Silicone oil bath at 200 °C. Vickers hardness of the samples was measured at certain time intervals by a Wilson Tukon 200 hardness tester under 1000 g of load applied for 15 s. At least six measurements were done and the average and standard deviation was reported at each point. A sample of T5 alloy was taken out from aging bath at the same time that T5–0.8Hf and T5–1.5Hf samples reached their peak hardness for better comparison.

Table 1
Nominal compositions of the Mg–Sn–Hf alloys; balance is Mg.

Alloy designation	Atomic percent		Weight percent	
	Sn	Hf	Sn	Hf
T5	1.1	–	5.15	–
T5–0.8Hf	1.1	0.11	5.12	0.77
T5–1.5Hf	1.1	0.22	5.08	1.53
T10	2.2	–	9.9	–
T10–0.7Hf	2.2	0.11	9.84	0.74
T10–1.5Hf	2.2	0.22	9.77	1.47

For microstructural studies, samples were mechanically ground with 600 and 1200 SiC papers, and then polished with alumina particles down to 0.03 μm. After polishing, samples were etched in Nital solution.

A FEI™ TEM200 Focused Ion Beam (FIB) with Gallium ion source was employed to obtain TEM thin foils. TEM was done by a Phillips CM-200 operating at 200 kV. Three different areas of the samples were used to calculate the number density of the precipitates in unit volume. STEM characterization was carried out using a FEI/Tecnai™ F30 300 kV TEM equipped with a Fischione™ high angle annular dark field (HAADF) detector and an X-ray Energy Dispersive Spectroscopy (XEDS) detector.

3. Results and discussion

Fig. 1 shows the optical micrographs of microstructure of T5 at 77 h, T5–0.8Hf, and T5–1.5Hf at peak hardness. The average grain size was measured according to Heyn Lineal Intercept method (ASTM E112-96) and was 231 ± 91 μm for T5, 211 ± 75 μm for T5–0.8Hf, and 367 ± 139 μm for T5–1.5Hf.

Fig. 2 shows the age hardening behavior of the alloys at 200 °C. The most significant feature of both graphs is the reduction of time to reach peak hardness. The sluggish precipitate formation process in T5 was expedited by an order of magnitude, reducing from about 900 h to 77 h in T5–0.8Hf and T5–1.5Hf. In T10 binary alloy, peak hardness occurs after 220 h of aging, which is reduced to 49 and 96 h in T10-0.7Hf and T10-1.5Hf respectively. Also, the maximum hardness was improved by Hf additions. As can be seen, the initial hardness of Hf containing samples are either close or lower than binary alloys. However, the addition of 0.1 at% Hf improves the percent increase in hardness from a mere 19% to 28.6% in T5–0.8Hf. In T5–1.5Hf, a 37.3% increase was observed, almost a two-fold increase over the binary T5 alloy. The percent increase in hardness in Hf modified T10 alloys are also improved from 35.4% to 41.8% and 44.9% in T10-0.7Hf and T10-1.5Hf respectively. The

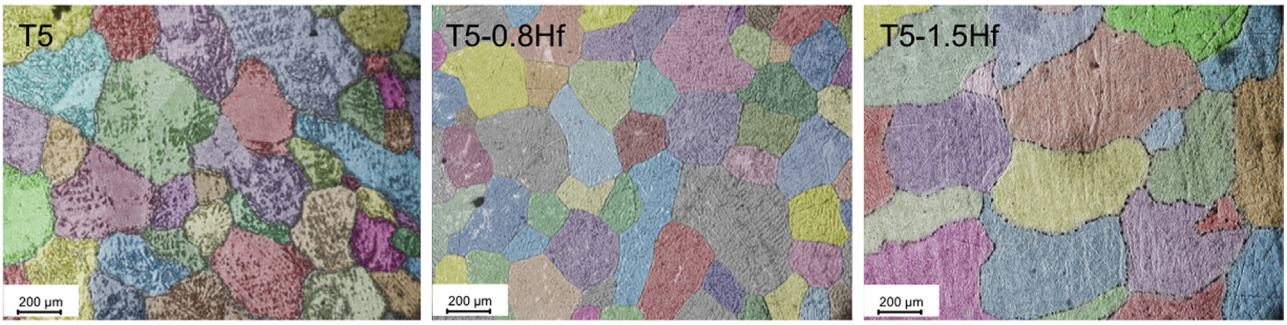

Fig. 1. Microstructure of the samples under optical microscope at peak hardness; (a)T5 after 77 h for comparison, (b)T5–0.8Hf, and (c)T5–1.5Hf.

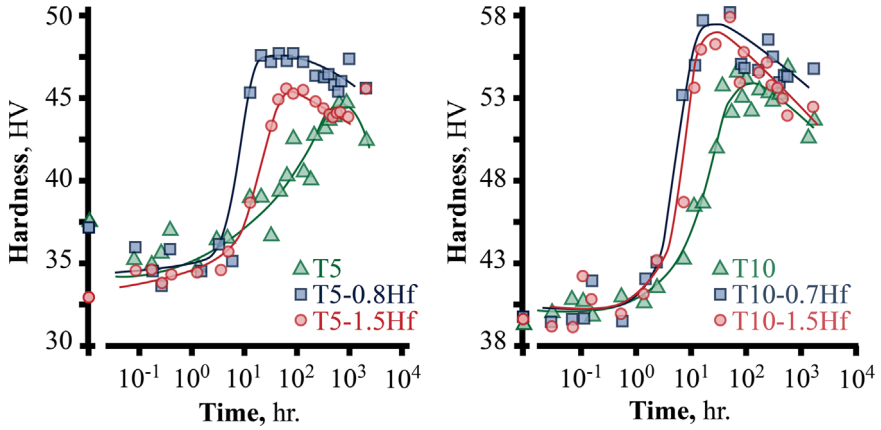

Fig. 2. Age hardening behavior of the alloys after artificial aging in Silicone oil at 200 °C; lines are added for clarity and are not true trendlines.

Table 2
Summary of ageing response of alloys at 200 °C.

Alloy composition (at%)	Time to peak hardness (h)	Initial hardness (VHN)	Max. hardness (VHN)	Max. Increment in hardness (VHN)	Percent increase in hardness
Mg–1.1Sn (T5)	900	37.4 ± 3.7	44.5 ± 0.6	7.1	19.0
Mg–1.1Sn–0.11Hf (T5–0.8Hf)	77	37.1 ± 3.8	47.7 ± 1.0	10.6	28.6
Mg–1.1Sn-0.22Hf (T5–1.5Hf)	77	32.7 ± 1.9	44.9 ± 1.5	12.2	37.3
Mg–2.2Sn (T10)	220	39.8 ± 4.2	53.9 ± 2.2	14.1	35.4
Mg–2.2Sn–0.11Hf (T10-0.7Hf)	49	40.2 ± 2.5	57.0 ± 2.4	16.8	41.8
Mg–2.2Sn-0.22Hf (T10-1.5Hf)	96	40.1 ± 2.3	58.1 ± 1.5	18.0	44.9

observed improvement in precipitate formation kinetics is in good agreement with previous studies [27,30], where micro-alloying with Na decreased time to reach peak hardness. Results are summarized in Table 2 for easier comparison. To explore the mechanism of the observed improvements, T5–0.8Hf and T5–1.5Hf were chosen for further analysis.

Bright-field TEM pictures of samples are shown in Fig. 3 (Table 3). Previous studies have reported lath shaped, plate like and polygon Mg_2Sn precipitates in Mg–Sn alloys [26–29,35,36]. In T5–0.8Hf and T5–1.5Hf, lath shaped precipitates can clearly be seen. The length of these lath-like precipitates reaches to several hundred nanometers (Fig. 3.c, e). In T5 binary alloy, only polygon shaped precipitates of very small size (less than 20 nm) were formed at the same timescales. The aspect ratio of the precipitates is increased to 3.63 and 3.95 in T5–0.8Hf and T5–1.5Hf respectively as compared to an aspect ratio of 1.42 in T5 alloy. Number volume density of precipitates was also increased to 41.2×10^{18} in T5–0.8Hf and 50.4×10^{18} in T5–1.5Hf per m^{-3}. Previous studies on Mg–1.3Sn reported a number volume density of 0.60×10^{18} per m^{-3} at its peak hardness which is two orders of magnitude lesser than the values found for Hf modified alloys in this study [27,28].

Clusters of Hf as dark spots at the surface of the precipitates in Hf modified alloys were seen in bright field TEM images. Elemental maps in Fig. 4 suggest the presence of these clusters at the surface and in the vicinity of precipitates by low magnification STEM and X-ray Energy Dispersive Spectroscopy (XEDS). The positive enthalpy of mixing between Mg and Hf ($\Delta H = +10$ kJ mole^{-1}) [37], as evidenced by virtually zero solubility in Hf–Mg phase diagram, acts as a driving force for Hf to segregate out even at such small concentrations. These Hf clusters have a negative enthalpy of mixing with Sn atoms ($\Delta H = -35$ kJ mole^{-1}) [37], and can form co-segregates as shown in Fig. 4(g). Co-segregated clusters act as additional nucleation centers for Mg_2Sn formation, hence leading to improvement of aging kinetics and precipitate size refinement. The significant difference in precipitate state in T5–0.8Hf and T5 can clearly be seen by comparison HAADF images in Fig. 4(e) and (f).

Microalloying with 0.1 at% Zn is shown to increase the hardness of T10 alloy by almost 43% (ΔHV ~ 21.4) [26], which is very close to 41.8% improvement observed by similar Hf additions in Mg–2.2Sn–0.11Hf (Table 2). Time to reach peak hardness was also reported to decrease from about 390 h to 130 h which is comparable to the reduction observed in Hf modified T10 alloys. Mendis et al. [27,28] reported that Mg–1.3Sn–1.2Zn and Mg–1.3Sn–0.12 Na both showed 75% increase in hardness (ΔHV ~ 30 and 26.8 respectively)

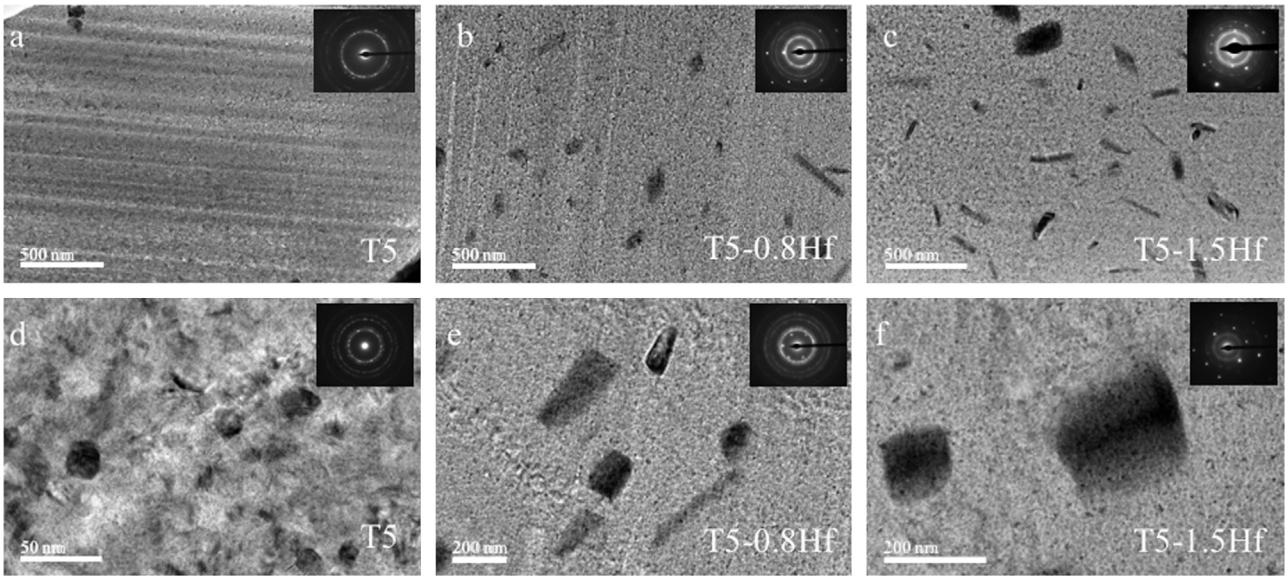

Fig. 3. Bright-field TEM pictures showing precipitates in peak-aged alloys; a) and d) show T5 at 77 h; (b) and (e) T5–0.8Hf at 77 h; (c) and (f) T5–1.5Hf at 77 h of artificial aging at 200 °C.

Table 3
Precipitate dimensions in peak-aged Hf modified alloys and T5 at 77 h.

Alloy	N_v x 10^{18} (m^{-3})	Length (nm)	Width (nm)	L/W
T5–0.8Hf	41.20	138 ± 34	38 ± 18	3.63
T5–1.5Hf	50.40	170 ± 56	43 ± 21	3.95
T5 at 77 h	NA[a]	17 ± 7	12 ± 4	1.42

[a] Due to the small size of the precipitates in T5 alloy, we were unable to calculate number volume density of precipitates in T5 sample in low magnification pictures. Values calculated from high magnification images are not reported, because it won't be a true measure of precipitate state at bulk.

in artificial ageing at 200 °C. Time to reach peak hardness was reduced from ~1000 h in Mg–1.3Sn alloy to 211 and 58 h for Zn and Na modified alloys respectively. Microalloying with Na and Hf, at about one order of magnitude lower atomic percentage, is much more effective than Zn in reduction of time to reach peak hardness. This is partly due to higher solid solubility of Zn in Mg [38]. It is believed that Na acts by increasing the number density of precipitates, while Zn additions change the particle morphology with respect to basal planes. Figs. 4(g) and 2(f) clearly show co-segregated nano-clusters of Hf at the surface of a precipitate in peak-

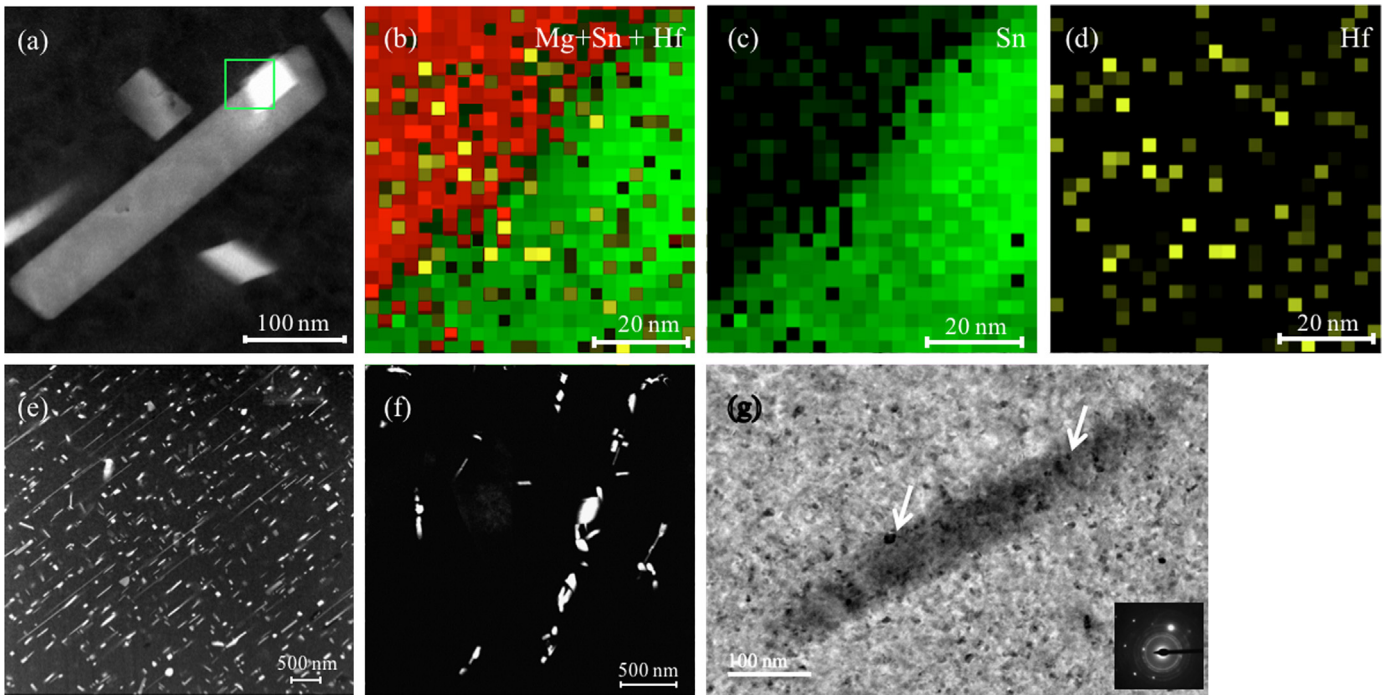

Fig. 4. (a) Low magnification STEM image of T5–0.8Hf alloy peak aged at 200 °C, and EDX mapping of green box showing (b) Mg (red)+Sn+Hf superimposed map, (c) Sn distribution (green), and (d) Hf distribution (yellow). (e) HAADF image of precipitates in peak-aged T5–0.8Hf, and (f) HAADF image of precipitates in T5 after 77 h at 200 °C, (g) nano-clusters of Hf at the surface of a precipitate in peak-aged T5–0.8Hf. (For interpretation of the references to color in this figure legend, the reader is referred to the web version of this article.)

aged T5–0.8Hf and T5–1.5Hf respectively. Microalloyed Hf acts similar to Na addition, forming nano-clusters that improve the ageing response by providing additional heterogeneous nucleation centers for Mg_2Sn formation.

4. Conclusion

In summary, micro-alloying Mg–5Sn with Hafnium leads to both higher increase in hardness and lesser time to reach peak hardness. Hafnium addition follows the criterion proposed by Mendis et al. [27]. Average size of the precipitates was 8–10 times larger and their aspect ratio was increased by ~2.5 times more than unmodified binary alloy aged for the same time at 200 °C. The presence of Hf clusters at the surface of precipitates is an indication that Hafnium addition acts through same pathways as Na. These microalloyed compositions exhibit better aging kinetics due to precipitate refinement and show promise for development of both die-cast and age-hardenable wrought Mg–Sn alloys.

Novelty statement

This study presents fabrication of novel Mg–Sn–Hf ternary alloys that exhibit significantly accelerated aging kinetics *(from 1000 h to less than 100 h)* and enhanced peak hardness. The present study proposes novel compositions that has never been synthesized and provides experimental evidence to validate the formation of Hafnium nano-clusters, which leads to improvement in aging kinetics. Results show excellent agreement between the proposed mechanism and experimental observations using multiple analytical techniques, including high resolution TEM.

Acknowledgment

Authors acknowledge Advanced Materials Engineering Research Institute (AMERI) and Dr. Yusuf Emirov for conducting TEM experiments. SB acknowledges Florida International University Graduate School for Dissertation Year Fellowship (DYF). SB would like to thank Dr. Ali Karbasi, Dr. K.W. Jones, Dr. C.C. Kammerer and A. Hadjikhani for their helpful discussions. MVM would like to thank the National Science Foundation for their support under DMR – 0845868.

References

[1] M.M. Avedesian, H. Baker, ASM Specialty Handbook: Magnesium and Magnesium Alloys, 1999.
[2] A. Ditze C. Scharf Recycling of Magnesium, 2008.
[3] M. Easton, A. Beer, M. Barnett, C. Davies, G. Dunlop, Y. Durandet, S. Blacket, T. Hilditch, P. Beggs, J. Oper. Manag. 60 (2008) 57.
[4] A.A. Luo, Recent magnesium alloy development for automotive powertrain applications, Mater. Sci. Forum 419 (2003) 57–66.
[5] E. Aghion, B. Bronfin, Magnesium alloys development towards the 21st century, Mater.Sci.Forum 350 (2000) 19.
[6] J. Nie, B. Muddle, Scr. Mater. 40 (1999) 1089.
[7] H. Furuya, N. Kogiso, S. Matunaga, K. Senda, Applications of magnesium alloys for aerospace structure systems, Mater.Sci.Forum 350 (2000) 341–348.
[8] I.S. Berglund, H.S. Brar, N. Dolgova, A.P. Acharya, B.G. Keselowsky, M. Sarntinoranont, M.V. Manuel, J. Biomed. Mater. Res. B: Appl. Biomater. 100 (2012) 1524.
[9] N.T. Kirkland, N. Birbilis, J. Walker, T. Woodfield, G.J. Dias, M.P. Staiger, J. Biomed. Mater. Res. B: Appl. Biomater. 95 (2010) 91.
[10] N. Kirkland, J. Lespagnol, N. Birbilis, M. Staiger, Corros. Sci. 52 (2010) 287.
[11] H.S. Brar, J. Wong, M.V. Manuel, J. Mech. Behav. Biomed. Mater. 7 (2012) 87.
[12] A.A. Luo, Int. Mater. Rev. 49 (2004) 13.
[13] K. Braszczyńska-Malik, J. Alloy. Compd. 477 (2009) 870.
[14] B.R. Powell, V. Rezhets, M.P. Balogh, R.A. Waldo, J. Oper. Manag. 54 (2002) 34.
[15] I. Moreno, T. Nandy, J. Jones, J. Allison, T. Pollock, Scr. Mater. 48 (2003) 1029.
[16] S. He, L. Peng, X. Zeng, W. Ding, Y. Zhu, Mater. Sci. Eng.: A 433 (2006) 175.
[17] H. Zhou, Z. Zhang, C. Liu, Q. Wang, Mater. Sci. Eng.: A 445 (2007) 1.
[18] J. Zhang, Q. Ma, F. Pan, Mater. Des. 31 (2010) 4043.
[19] Q. Chen, D. Shu, Z. Zhao, Z. Zhao, Y. Wang, B. Yuan, Mater. Des. 40 (2012) 488.
[20] E. Aghion, B. Bronfin, F. Von Buch, S. Schumann, H. Friedrich, J. Oper. Manag. 55 (2003) 30.
[21] H.E. Friedrich, B.L. Mordike, Magnesium Technology, Springer, Berlin, Germany, 2006.
[22] J. Wang, L. Hsiung, T. Nieh, M. Mabuchi, Mater. Sci. Eng.: A 315 (2001) 81.
[23] S.R. Agnew, J. Oper. Manag. 56 (2004) 20.
[24] N. Hort, Y. Huang, K.U. Kainer, Adv. Eng. Mater. 8 (2006) 235.
[25] J. Nie, Metall. Mater. Trans. A 43 (2012) 3891.
[26] T. Sasaki, K. Oh-Ishi, T. Ohkubo, K. Hono, Scr. Mater. 55 (2006) 251.
[27] C. Mendis, C. Bettles, M. Gibson, S. Gorsse, C. Hutchinson, Philos. Mag. Lett. 86 (2006) 443.
[28] C. Mendis, C. Bettles, M. Gibson, C. Hutchinson, Mater. Sci. Eng.: A 435 (2006) 163.
[29] C. Mendis, K. Oh-Ishi, K. Hono, Scr. Mater. 57 (2007) 485.
[30] F. Elsayed, T. Sasaki, C. Mendis, T. Ohkubo, K. Hono, Mater. Sci. Eng.: A 566 (2013) 22.
[31] X. Huang, W. Zhang, Y. Ma, M. Yin, Philos. Mag. Lett. 94 (2014) 460.
[32] H. Okamoto, J. Phase Equilib. 12 (1991) 472.
[33] B. Predel, O. Madelung, The Landolt-Börnstein Databas, Landolt-Börnstein-Group IV Physical Chemistry Volume 5f, SpringerMaterials, 1996.
[34] H. Liu, Y. Chen, Y. Tang, S. Wei, G. Niu, J. Alloy. Compd. 440 (2007) 122.
[35] T. Sasaki, K. Oh-Ishi, T. Ohkubo, K. Hono, Mater. Sci. Eng.: A 530 (2011) 1.
[36] X. Nie, Y. Guan, D. Zhao, Y. Liu, J. Gui, L. Li, J. Wang, J. Appl. Crystallogr. 47 (2014) 1729.
[37] F.R. De Boer, R. Boom, W.C.M. Mattens, A.R. Miedema, A.K. Niessen, Cohesion in metals: transition metal alloys, North-Holland, Amsterdam, 1988. For Reference ISBN-13: 978-0444870988.
[38] C.C. Kammerer, S. Behdad, L. Zhou, F. Betancor, M. Gonzalez, B. Boesl, Y. H. Sohn, Intermetallics 67 (2015) 145.